pp 1437–1453. © Royal Aeronautical Society 2019
doi:10.1017/aer.2019.71

Adaptive integrated guidance and control for impact angle constrained interception with actuator saturation

X. L. Ai
bitaixiaolin@163.com
School of Aerospace Engineering
Beijing Institute of Technology
Beijing, 100081, China

Y. C. Shen
Beijing Institute of Electronic System Engineering
Beijing, 100854, China

L. L. Wang
Beijing Institute of Space Long March Vehicle
Beijing, 100076, China

ABSTRACT

This paper considers the integrated guidance and control (IGC) problem for impact angle constrained interception against manoeuvring targets with actuator saturation constraint. Based on the backstepping technique, an adaptive IGC law is presented to address this problem, where a fixed-time differentiator is proposed to estimate the derivatives of virtual control inputs to avoid the inherent problem of "explosion of complexity" suffered by the typical backstepping. Furthermore, an auxiliary first-order filter is introduced into the IGC law to cope with the actuator saturation constraint. The stability of the closed-loop system is strictly proved. Finally, the superiority of the proposed IGC law is verified by comparison simulations.

Keywords: Integrated guidance and control; Impact angle constraint; Actuator saturation; Aerodynamic uncertainties; Manoeuvring targets

NOMENCLATURE

a_M, a_T $\left(\mathrm{m/s^2}\right)$	missile and target accelerations
g $\left(\mathrm{m/s^2}\right)$	acceleration due to gravity
J_z $\left(\mathrm{kg \bullet m^2}\right)$	moment of inertia
L (m)	reference length

Received 6 September 2018; revised 9 January 2019; accepted 24 June 2019.

L_f (N)	aerodynamic lift force
M (N • m)	aerodynamic pitch moment
m (kg)	missile mass
Q $\left(\text{kg/m/s}^2\right)$	dynamic pressure
r (m)	relative distance
S $\left(\text{m}^2\right)$	reference area
V_M, V_T (m/s)	missile and target velocities
α (rad)	angle-of-attack
δ_z (rad)	fin deflection angle
γ_M, γ_T (rad)	missile and target flight-path angles
λ (rad)	line-of-sight angle
ϑ (rad)	pitch angle
ω_z (rad/s)	pitch angular rate

1.0 INTRODUCTION

Owing to the requirements of modern wars, guidance and control system design has remained a technical area of active research for tactical missiles during the past several decades. Usually, the guidance and control systems can be considered separately by neglecting their coupling effect, resulting in a typically-used hierarchical two-loop control scheme[1,2]. Concerning this methodology, a variety of efficient guidance laws, ranging from proportional navigation guidance (PNG)[3,4] to robust control algorithms[5–7] have been reported in literature. Thereafter, wide attention has focused on impact angle constrained guidance to improve the killing efficiency of missiles. The impact angle can be defined as the intersect angle between the velocity vectors of the missile and the target when the interception is achieved. As the target's motion generally remains uncertain in practical applications, sliding mode control (SMC) has been widely utilised in impact angle control against manoeuvring targets. Authors of[8] presented a linear sliding surface to construct an impact angle constrained guidance law for both head-on and tail-chase scenarios. To realise the finite-time convergence, terminal sliding mode (TSM) technique was adopted in[9] to address the impact angle constrained guidance law design problem, and a non-singular TSM (NTSM) algorithm was further proposed in[10] to avoid the singularity problem suffered by TSM. One drawback of the guidance laws in[9,10] is that the settling time relies on the initial conditions, which may not be easily obtained in practical applications. To cope with this problem, an extension of the finite-time stability, named fixed-time stability, was utilised in impact angle constrained guidance law design in[11,12], featuring a predesigned convergence time regardless of the initial conditions. Although the aforementioned guidance laws have been successfully applied in target interception, the performance of the two-loop control scheme may seriously degrade when intercepting highly manoeuvring targets[13].

To improve the kill envelope of missiles, the integrated guidance and control (IGC) concept has become an emerging trend. Generally, existing IGC laws can fall into either the autopilot compensation-based guidance or the fully IGC law[13]. For the former guidance scheme, the autopilot is usually assumed to be a first-order or second-order dynamics, and then compensation is added into the guidance law design to handle the time lag of the autopilot[14–17]. However, accurate estimation of the autopilot cannot be achieved in practical applications due to inevitable uncertainties of aerodynamics. With this in mind, the fully IGC law, which is obtained from the complete guidance and control system, has attracted significant attention in the most recent period. Some control approaches including feedback linearization[18],

https://doi.org/10.1017/aer.2019.71 Published online by Cambridge University Press

state-dependent Riccati equation (SDRE) method[19], $\theta - D$ method[20], model predictive static programming approach[21] and finite horizon optimal control[22] have contributed to the development of the IGC law design. However, these IGC laws all involve complicated numerical computations, and the robustness of the closed-loop system cannot be guaranteed[23]. To enhance the robustness of the closed-loop system, SMC-based IGC laws were reported in[24,25], in which the sliding surfaces were designed to null the line-of-sight angular velocity.

Besides the above approaches, backstepping is widely accepted in the IGC law design as the guidance and control system performs in a strict-feedback form[26,27]. However, an obvious drawback for using the backstepping technique is the problem of 'explosion of complexity', which is caused by repeated differentiation of the virtual control input in each step[28]. To tackle this problem, a so-called dynamic surface control (DSC) technique has been utilised to develop IGC laws. In[29], an adaptive block DSC algorithm was carried out to design an IGC law, which is only suitable for attacking weak manoeuvrable targets. Authors of[30] presented an adaptive fuzzy DSC-based IGC law in which a fuzzy system was introduced to estimate and compensate lumped uncertainties. Nonetheless, this algorithm is somewhat complicated, and the introduced fuzzy system may significantly raise computation time. To simplify the IGC law design, authors in[31] proposed a smooth second-order sliding mode (SSOSM) differentiator to estimate the derivatives of the virtual control inputs, based on which an impact angle constrained IGC law was proposed with the consideration of aerodynamic uncertainties. One drawback of the aforementioned results is that the actuator saturation constraint is not taken into account in the IGC law design. Because the actuator saturation may severely degrade the performance of the guidance and control system, it has practical significance for studying IGC law design with actuator saturation.

Motivated by the aforementioned observation, the full impact angle constrained IGC law design problem with actuator saturation constraint and aerodynamic uncertainties is considered in this study for manoeuvring target interception. The target acceleration and aerodynamic uncertainties are considered as lumped disturbances, which are compensated by a proposed adaptation law in the IGC law design. Then, the backstepping approach is utilised to carry out the IGC law, where a fixed-time differentiator is presented to avoid the problem of 'explosion of complexity'. Additionally, an auxiliary fist-order filter is proposed to cope with the actuator saturation problem. The major contributions of this study can be summarised as follows: 1) the proposed IGC law does not require any information within the bounds of both the target acceleration and uncertain aerodynamics; 2) the difficulty arises from the stability analysis in the presence of actuator saturation; 3) both the aerodynamic uncertainties and actuator saturation constraint taken into consideration generally broadens practical applications of proposed IGC law, which is significantly different from existing IGC algorithms.

The rest of this paper is organised as follows. The problem formulation is presented in Section 2. Section 3 gives the proposed IGC law together with the stability analysis in detail. In Section 4, comparison examples are illustrated, and the simulation results are also provided. Finally, conclusions are drawn in Section 5.

2.0 PROBLEM FORMULATION

This study considers the impact angle constrained IGC law design problem within the perpendicular plane. Figure 1 depicts a schematic view of 2D planar homing engagement geometry, where V_M and V_T are missile and target velocities satisfying $V_T/V_M > 1$, a_M and a_T are missile and target accelerations being normal to their corresponding velocities, γ_M and γ_T are

https://doi.org/10.1017/aer.2019.71 Published online by Cambridge University Press

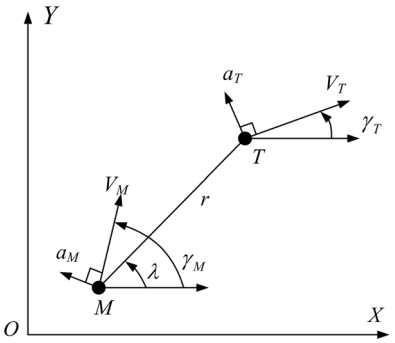

Figure 1. Planar engagement geometry.

missile and target flight-path angles and r and λ denote the relative range between the missile and the target and the line-of-sight (LOS) angle, respectively. For simplicity, the missile and the target are regarded as point masses moving with constant velocities.

The corresponding kinematic engagement equations describing the relative motion between the target and the missile can be formulated as[31]

$$\dot{r} = V_T \cos(\lambda - \gamma_T) - V_M \cos(\lambda - \gamma_M) \quad \ldots (1)$$

$$r\dot{\lambda} = V_T \sin(\gamma_T - \lambda) - V_M \sin(\gamma_M - \lambda) \quad \ldots (2)$$

$$\dot{\gamma}_M = \frac{a_M}{V_M} \quad \ldots (3)$$

$$\dot{\gamma}_T = \frac{a_T}{V_T} \quad \ldots (4)$$

Let $V_\lambda = r\dot{\lambda}$ and differentiating Equations (1) and (2) with respect to time yields that

$$\ddot{r} = r\dot{\lambda}^2 - a_M \sin(\lambda - \gamma_M) + a_T \sin(\lambda - \gamma_T) \quad \ldots (5)$$

$$\dot{V}_\lambda = a_T \cos(\gamma_T - \lambda) - a_M \cos(\gamma_M - \lambda) - \dot{r}\dot{\lambda} \quad \ldots (6)$$

Generally, the acceleration along the missile's velocity cannot be controlled in the terminal guidance phase; hence, only the second-order dynamics between the missile's normal acceleration a_M and the LOS angle λ is utilised to address the IGC problem in the terminal guidance phase[32,33].

The missile considered in this study is an aerodynamically controlled vehicle, and the planar dynamics can be given by[31]

$$\begin{cases} \dot{\alpha} = \dfrac{1}{mV_M}\left(-L_f + mg\cos\gamma_M\right) + \omega_z \\ \dot{\omega}_z = \dfrac{M_z}{J_z} \\ \dot{\vartheta} = \omega_z \\ \alpha = \vartheta - \gamma_M \end{cases} \quad \ldots (7)$$

https://doi.org/10.1017/aer.2019.71 Published online by Cambridge University Press

in which m is the missile mass, α denotes the angle-of-attack, g is the acceleration due to gravity, J_z is the moment of inertia, ω_z represents the pitch angular rate and ϑ is the pitch angle. Besides, L_f and M_z, representing the aerodynamic lift force and pitch moment without considering direct aerodynamic force from the control surfaces, can be modelled as[31]

$$\begin{cases} L = QSc_y^{\alpha}\alpha \\ M_z = QSLm_z^{\alpha}\alpha + \dfrac{QSL^2 m_z^{\omega_z}}{V_M}\omega_z + QSLm_z^{\delta_z}\text{sat}\,(\delta_z) \end{cases} \quad \ldots (8)$$

where Q denotes the dynamic pressure, S denote the reference area, L is the reference length and δ_z is the actuator deflection angle under the following saturation constraint

$$\text{sat}\,(\delta_z) = \begin{cases} \delta_z & \text{if } |\delta_z| \le \delta_{\max} \\ \delta_{\max} sign\,(\delta_z) & \text{if } |\delta_z| > \delta_{\max} \end{cases} \quad \ldots (9)$$

with $\delta_{\max}$ being the upper bound. The notation c_y^{α} is the lift force co-efficient derivative with respect to α. Similarly, m_z^{α}, $m_z^{\omega_z}$, and $m_z^{\delta_z}$ are the pitch moment co-efficient derivatives with respect to α, ω_z, and δ_z.

Because of Equations (7) and (8), the missile acceleration can be rewritten as[31]

$$a_M = V_M\dot{\gamma}_M = \frac{QSc_y^{\alpha}\alpha}{m} - g\cos\gamma_M \quad \ldots (10)$$

In practical applications, the precise values of the aforementioned aerodynamic parameters cannot be measured in wind-tunnel experiments. Therefore, it is necessary and reasonable to take aerodynamic uncertainties into consideration in IGC design, and then the aforementioned aerodynamic parameters can be further formulated as[31]

$$\begin{aligned} c_y^{\alpha} &= c_{y,n}^{\alpha} + c_{y,u}^{\alpha} \quad m_z^{\alpha} = m_{z,n}^{\alpha} + m_{z,u}^{\alpha} \\ m_z^{\omega_z} &= m_{z,n}^{\omega_z} + m_{z,u}^{\omega_z}\; m_z^{\delta_z} = m_{z,n}^{\delta_z} + m_{z,u}^{\delta_z} \end{aligned} \quad \ldots (11)$$

where the parameters with subscripts n and u indicate the nominal values and uncertain values, respectively.

Usually, the impact angle can be defined as the intersect angle between the velocity vectors of the missile and the target when the interception is achieved[34]. Hence, the IGC law considered in this study tries to obtain precise target capture with a desired impact angle γ_d, that is

$$\gamma_d = \gamma_T\left(t_f\right) - \gamma_M\left(t_f\right) \quad \ldots (12)$$

where t_f is the interception time. As indicated in[35] that for a perfect interception (e.g., $\dot{\lambda} = V_{\lambda} = 0$) with an expected impact angle, there always exists a unique desired LOS angle λ_d, which can be obtained by[35]

$$\lambda_d = \gamma_T - \text{atan2}\left(\frac{\sin\gamma_d}{\cos\gamma_d - V_T/V_M}\right) \quad \ldots (13)$$

where atan2 is the arctangent function returning the angle in its appropriate quadrant. Hence, the control objective of the impact angle constrained IGC problem considered in this paper

https://doi.org/10.1017/aer.2019.71 Published online by Cambridge University Press

can be stated as designing an IGC law for δ_z, such that the manoeuvring target interception can be achieved with a desired LOS angle in the presence of aerodynamic uncertainties with actuator saturation constraint.

Remark 1. *As pointed out in [11,12], the target flight-path angle γ_T can always be measured or predicted by a tracking filter no matter if the target is stationary or manoeuvring. Therefore, it is reasonable to assume that the value of γ_T is known in the IGC law design.*

3.0 IGC LAW DESIGN AND STABILITY ANALYSIS

3.1 IGC law design

In this section, a novel adaptive backstepping-based IGC law is presented to address the impact angle constrained IGC problem with actuator saturation. Before moving on, the following assumption is given firstly, which is usually utilised in the stability analysis.

Assumption 1. *There exist two positive constants $\bar{r}$ and $\underline{r}$, such that $\underline{r} < r < \bar{r}$ is satisfied during the overall guidance phase. Moreover, the lower bound $\underline{r}$ can be given according to the target physical size.*

With the above assumption in mind, the proposed IGC law will be given step by step in the following text.

Step 1: Let $s_1 = (\lambda - \lambda_d)/r$; differentiating s_1 with respect to time yields that

$$\dot{s}_1 = \frac{1}{r}\left(\frac{V_\lambda}{r} - \frac{\dot{r}(\lambda - \lambda_d)}{r} + \Delta_1\right) = \frac{1}{r}\left(\frac{V_\lambda^*}{r} + \frac{V_\lambda - V_\lambda^*}{r} - \frac{\dot{r}(\lambda - \lambda_d)}{r} + \Delta_1\right) \quad \ldots (14)$$

where V_λ^* denotes a virtual control input, and $\Delta_1 = -a_T/V_T$ is considered as an external disturbance with unknown upper bound d_1, that is $|\Delta_1| \leq d_1$. To stabilise the system shown in Equation (14), one can select the following virtual control input:

$$V_\lambda^* = -k_1(\lambda - \lambda_d) + \dot{r}(\lambda - \lambda_d) - \frac{r s_1 \hat{d}_1^2}{2\varepsilon_1} \quad \ldots (15)$$

where $k_1 > 0$ and $\varepsilon_1 > 0$ are design parameters, and $\hat{d}_1$ is the estimation of d_1 governed by the following adaptive law

$$\dot{\hat{d}}_1 = \frac{c_1 |s_1|}{r} - \sigma_1 \hat{d}_1 \quad \ldots (16)$$

with constants $c_1 > 0$ and $\sigma_1 > 0$.

Step 2: Let $s_2 = \left(V_\lambda - V_\lambda^*\right)/r$, differentiating s_2 based on Equations (6) and (7) with respect to time yields that

$$\dot{s}_2 = \frac{1}{r}\left[-\frac{QSc_{y,n}^\alpha \cos(\gamma_M - \lambda)}{m}\alpha - \dot{r}s_2 - \dot{\lambda}\dot{r} - \dot{V}_\lambda^* + g\cos\gamma_M \cos(\gamma_M - \lambda) + \Delta_2\right]$$

https://doi.org/10.1017/aer.2019.71 Published online by Cambridge University Press

$$= \frac{1}{r}\left[-\frac{QSc_{y,n}^{\alpha}\cos(\gamma_M-\lambda)}{m}\alpha^* - \frac{QSc_{y,n}^{\alpha}\cos(\gamma_M-\lambda)}{m}(\alpha-\alpha^*) - \dot{r}s_2 - \dot{\lambda}\dot{r} - \dot{V}_{\lambda}^* + g\cos\gamma_M\cos(\gamma_M-\lambda) + \Delta_2\right] \quad \ldots (17)$$

where α^* denotes a virtual control input, and $\Delta_2 = a_T\cos(\gamma_T-\lambda) - \frac{QSc_{y,u}^{\alpha}\alpha\cos(\gamma_M-\lambda)}{m}$ is considered as an external disturbance with unknown upper bound d_2, that is $|\Delta_2| \le d_2$. For the subsystem in Equation (17), select the following virtual control input:

$$\alpha^* = \frac{m}{QSc_{y,n}^{\alpha}\cos(\gamma_M-\lambda)}\left[-\dot{\lambda}\dot{r} - \dot{V}_{\lambda}^* + g\cos\gamma_M\cos(\gamma_M-\lambda) + k_2s_2 + s_1 + \frac{s_2\hat{d}_2^2}{2\varepsilon_2} - \dot{r}s_2\right] \quad \ldots (18)$$

where $k_2 > 0$ and $\varepsilon_2 > 0$ are design parameters, and $\hat{d}_2$ is the estimation of d_2 governed by the following adaptive law

$$\dot{\hat{d}}_2 = \frac{c_2|s_2|}{r} - \sigma_2\hat{d}_2 \quad \ldots (19)$$

with constants $c_2 > 0$ and $\sigma_2 > 0$.

Step 3: Let $s_3 = \alpha - \alpha^*$, and differentiating s_3 with respect to time yields that

$$\dot{s}_3 = \omega_z^* + \left(\omega_z - \omega_z^*\right) - \frac{QSc_{y.n}^{\alpha}\alpha}{mV_M} + \frac{g\cos\gamma_M}{V_M} + \Delta_3 - \dot{\alpha}^* \quad \ldots (20)$$

where ω_z^* denotes a virtual control input, and $\Delta_3 = -\frac{QSc_{y,u}^{\alpha}\alpha}{mV_M}$ is considered as an external disturbance with unknown upper bound d_3, that is $|\Delta_3| \le d_3$. For the subsystem in Equation (20), consider the following virtual control law:

$$\omega_z^* = -k_3s_3 + \frac{QSc_{y,n}^{\alpha}\cos(\gamma_M-\lambda)}{mr}s_2 + \frac{QSc_{y.n}^{\alpha}\alpha}{mV_M} - \frac{g\cos\gamma_M}{V_M} + \dot{\alpha}^* - \frac{s_3\hat{d}_3^2}{2\varepsilon_3} \quad \ldots (21)$$

where $k_3 > 0$ and $\varepsilon_3 > 0$ are design parameters, and $\hat{d}_3$ is the estimation of d_3 governed by the following adaptive law

$$\dot{\hat{d}}_3 = c_3|s_3| - \sigma_3\hat{d}_3 \quad \ldots (22)$$

with constants $c_3 > 0$ and $\sigma_3 > 0$.

Step 4: Let $s_4 = \omega_z - \omega_z^*$, and differentiating s_4 with respect to time yields that

$$\begin{aligned}\dot{s}_4 &= \frac{QSLm_{z,n}^{\delta_z}}{J_z}\text{sat}(\delta_z) + \frac{QSLm_{z,n}^{\alpha}\alpha}{J_z} + \frac{QSL^2m_{z.n}^{\omega_z}\omega_z}{J_zV_M} - \dot{\omega}_z^* + \Delta_4 \\ &= \frac{QSLm_{z,n}^{\delta_z}}{J_z}\delta_z + \frac{QSLm_{z,n}^{\alpha}\alpha}{J_z} + \frac{QSL^2m_{z.n}^{\omega_z}\omega_z}{J_zV_M} - \dot{\omega}_z^* + \Delta_4 + \frac{QSLm_{z,n}^{\delta_z}}{J_z}\bar{\delta}_z\end{aligned} \quad \ldots (23)$$

https://doi.org/10.1017/aer.2019.71 Published online by Cambridge University Press

where $\Delta_4 = \frac{QSLm_{z,u}^{\alpha}\alpha}{J_z} + \frac{QSL^2 m_{z,u}^{\omega_z}\omega_z}{J_z V_M} + \frac{QSLm_{z,u}^{\delta_z}\mathrm{sat}(\delta_z)}{J_z}$ is considered as an external disturbance with unknown upper bound d_4, that is $|\Delta_4| \le d_4$ and $\bar{\delta}_z = \mathrm{sat}(\delta_z) - \delta_z$ is utilised to deal with the input saturation. We pass $\bar{\delta}_z$ through a first-order filter with a time constant τ_δ to obtain a filtered virtual control δ_e:

$$\dot{\delta}_e = -\frac{1}{\tau_\delta}\delta_e + \left|\frac{QSLm_{z,n}^{\delta_z}}{J_z}\right|\bar{\delta}_z. \quad \ldots (24)$$

in which the design variable is selected as

$$\frac{1}{\tau_\delta} = k_\delta + \frac{\left|\frac{4QSLm_{z,n}^{\delta_z}}{J_z}\right||s_4|\left|\bar{\delta}_z\right| + \left(\frac{QSLm_{z,n}^{\delta_z}}{J_z}\right)^2\bar{\delta}_z^2}{4\delta_e^2 + \varphi(\delta_e)} \quad \ldots (25)$$

with $k_\delta > 0$ and $\varphi(\delta_e) = \begin{cases} 0 \text{ if } \delta_e \neq 0 \\ 1 \text{ if } \delta_e = 0 \end{cases}$.

For the subsystem in Equation (23), consider the following virtual control law:

$$\delta_z = \frac{J_z}{QSLm_{z,n}^{\delta_z}}\left(-k_4 s_4 - s_3 - \frac{QSLm_{z,n}^{\alpha}\alpha}{J_z} - \frac{QSL^2 m_{z,n}^{\omega_z}\omega_z}{J_z V_M} + \dot{\omega}_z^* - \frac{s_4\hat{d}_4^2}{2\varepsilon_4}\right) \quad \ldots (26)$$

where $k_4 > 0$ and $\varepsilon_4 > 0$ are design parameters, and $\hat{d}_4$ is the estimation of d_4 governed by the following adaptive law

$$\dot{\hat{d}}_4 = c_4|s_4| - \sigma_4\hat{d}_4 \quad \ldots (27)$$

with constants $c_4 > 0$ and $\sigma_4 > 0$.

The aforementioned presentation gives an IGC law design approach based on the typical backstepping design. It can be seen from Equations (18), (21) and (26) that the virtual control inputs' derivative $\dot{V}_\lambda^*$, $\dot{\alpha}^*$ and $\dot{\omega}_z^*$ are included in the IGC law, while these variables may not be easily acquired in reality, and an direct differential of V_λ^*, α^* and ω_z^* leads to the so-called "explosion of complexity" in the sequel. To cope with this problem, a fixed-time differentiator is proposed based on the result in[36] as a feasible way to reconstruct $\dot{V}_\lambda^*$, $\dot{\alpha}^*$ and $\dot{\omega}_z^*$ in the IGC law design. Accordingly, we have

$$\begin{cases} \dot{z}_1 = z_2 - \tau_1\left(|z_1 - z_d|^{a_1} + |z_1 - z_d|^{b_1}\right)\mathrm{sign}(|z_1 - z_d|) \\ \dot{z}_2 = -\tau_2\left(|z_1 - z_d|^{a_2} + |z_1 - z_d|^{b_2}\right)\mathrm{sign}(|z_1 - z_d|) \end{cases} \quad \ldots (28)$$

where z_d can be set as V_λ^*, α^* or ω_z^*, z_1 is the estimated value of z_d, z_2 is the estimated derivative of z_d corresponding to $\dot{V}_\lambda^*$, $\dot{\alpha}^*$ or $\dot{\omega}_z^*$, and τ_1, τ_2 are observer gains. Moreover, $a_1 \in (1-\upsilon, 1)$, $b_1 \in (1, 1+\upsilon)$, $a_2 = 2a_1 - 1$ and $b_2 = 2a_2 - 1$ where υ is a sufficiently small constant. It was indicated in[36] that, based on the differentiator Equation (28), the estimation errors are globally bounded and can converge to zero within a bounded finite time $T_{sd} > 0$. Considering this, the virtual control inputs presented in the aforementioned text can be transformed into the following form:

https://doi.org/10.1017/aer.2019.71 Published online by Cambridge University Press

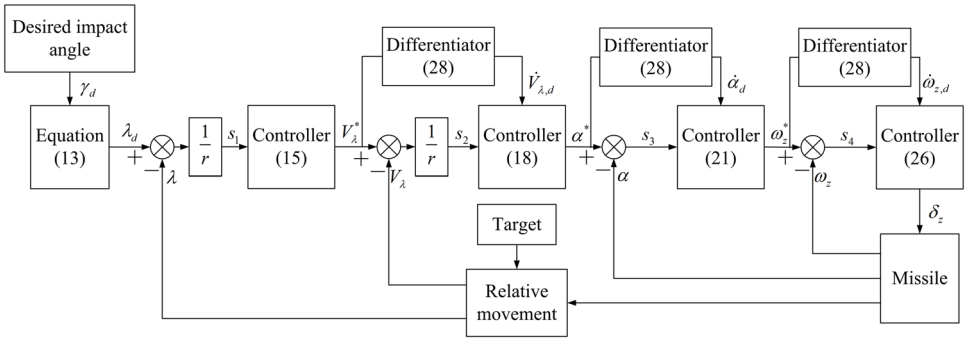

Figure 2. Controller structure.

$$
\begin{cases}
V_\lambda^* = -k_1(\lambda-\lambda_d) + \dot{r}(\lambda-\lambda_d) - \dfrac{rs_1\hat{d}_1^2}{2\varepsilon_1} \\
\alpha^* = \dfrac{m}{QSc_{y,n}^{\alpha}\cos(\gamma_M-\lambda)}\left[-\dot{\lambda}\dot{r} - \dot{V}_{\lambda,d} + g\cos\gamma_M\cos(\gamma_M-\lambda)\right. \\
\qquad\qquad \left. + k_2 s_2 + s_1 + \dfrac{s_2\hat{d}_2^2}{2\varepsilon_2} - \dot{r}s_2\right] \\
\omega_z^* = -k_3 s_3 + \dfrac{QSc_{y,n}^{\alpha}\cos(\gamma_M-\lambda)}{mr}s_2 + \dfrac{QSc_{y,n}^{\alpha}\alpha}{mV_M} \\
\qquad -\dfrac{g\cos\gamma_M}{V_M} + \dot{\alpha}_d - \dfrac{s_3\hat{d}_3^2}{2\varepsilon_3} \\
\delta_z = \dfrac{J_z}{QSLm_{z,n}^{\delta_z}}\left(-k_4 s_4 - s_3 + -\dfrac{QSLm_{z,n}^{\alpha}\alpha}{J_z} - \dfrac{QSL^2 m_{z,n}^{\omega_z}\omega_z}{J_z V_M} - \dfrac{s_4\hat{d}_4^2}{2\varepsilon_4} + \dot{\omega}_{z,d}\right)
\end{cases}
\quad \ldots (29)
$$

where $\dot{V}_{\lambda,d}$, $\dot{\alpha}_d$ and $\dot{\omega}_{z,d}$ are the estimations of $\dot{V}_\lambda^*$, $\dot{\alpha}^*$ and $\dot{\omega}_z^*$, respectively, and can be obtained based on the fixed-time differentiator in Equation (28). The overall controller structure is shown in Fig. 2.

Remark 2. *In the typical DSC design, a first-order filter is commonly used to cope with the 'explosion of complexity' problem, where a sufficiently small time constant is required to obtain fast and precise estimation leading to the peaking phenomenon during the initial moment. Compared with the typical DSC design, the fixed-time differentiator in Equation* (28) *can avoid this unexpected phenomenon efficiently.*

Remark 3. *By using the adaptation laws in Equations* (16), (19), (22) *and* (27)*, the upper bounds of the target acceleration and the uncertain aerodynamics are not required in the proposed IGC law, which helps to broaden the scope of practical applications. Moreover, the* $\sigma-$modification *terms are introduced in Equations* (16), (17), (22) *and* (27) *to avoid the over-estimation of uncertain parameters. This contributes to improve the steady-state performance of the closed-loop system.*

https://doi.org/10.1017/aer.2019.71 Published online by Cambridge University Press

3.2 Stability analysis

Based on the above analysis, the closed-loop system can be rewritten as

$$\begin{cases} \dot{s}_1 = \dfrac{1}{r}\left(-k_1 s_1 + \Delta_1 - \dfrac{s_1\hat{d}_1^2}{2\varepsilon_1} + s_2\right) \\ \dot{s}_2 = \dfrac{1}{r}\left(-k_2 s_2 + \Delta_2 - \dfrac{s_2\hat{d}_2^2}{2\varepsilon_2} - s_1 - \dfrac{QSc_{y,n}^{\alpha}\cos(\gamma_M - \lambda)}{m}s_3 + \dot{V}_{\lambda,d} - \dot{V}_{\lambda}^{*}\right) \\ \dot{s}_3 = -k_3 s_3 + \Delta_3 - \dfrac{s_3\hat{d}_3^2}{2\varepsilon_3} + \dfrac{QSc_{y,n}^{\alpha}\cos(\gamma_M - \lambda)}{mr}s_2 + s_4 + \dot{\alpha}_d - \dot{\alpha}^{*} \\ \dot{s}_4 = -k_4 s_4 - s_3 + \Delta_4 - \dfrac{s_4\hat{d}_4^2}{2\varepsilon_4} + \dot{\omega}_{z,d} - \dot{\omega}_z^{*} + \dfrac{QSLm_{z,n}^{\delta_z}}{J_z}\bar{\delta}_z \end{cases} \quad \ldots (30)$$

Next, the following theorem is given to show the main results achieved in this study.

Theorem 1. *For the error systems in Equation (30) with the adaptation laws of Equations (16), (19), (22) and (27) and the fixed-time differentiator in Equation (28), the closed-loop errors can be stabilised in the arbitrarily small neighbourhood of the origin.*

Proof . Consider the following Lyapunov candidate:

$$V = \frac{1}{2}\sum_{i=1}^{4} s_i^2 + \frac{1}{2c_i}\sum_{i=1}^{4}\tilde{d}_i^2 + \frac{1}{2}\delta_e^2 \quad \ldots (31)$$

where $\tilde{d}_i = d_i - \hat{d}_i$ $(i = 1, ..., 4)$ denote the estimation error of the lumped disturbance. □

Differentiating V with respect to time along trajectories, Equation (30) yields:

$$\begin{aligned} \dot{V} &= \sum_{i=1}^{4} s_i\dot{s}_i - \frac{1}{c_i}\sum_{i=1}^{4}\tilde{d}_i\dot{\hat{d}}_i + \delta_e\dot{\delta}_e \\ &= \frac{1}{r}\left(-k_1 s_1^2 - \frac{s_1^2\hat{d}_1^2}{2\varepsilon_1} + s_1\Delta_1 - \tilde{d}_1|s_1|\right) + \frac{1}{r}\left(-k_2 s_2^2 - \frac{s_2^2\hat{d}_2^2}{2\varepsilon_2} + s_2\Delta_2 - \tilde{d}_2|s_2|\right) \\ &\quad + \left(-k_3 s_3^2 - \frac{s_3^2\hat{d}_3^2}{2\varepsilon_3} + s_3\Delta_3 - \tilde{d}_3|s_3|\right) + \left(-k_4 s_4^2 - \frac{s_4^2\hat{d}_4^2}{2\varepsilon_4} + s_4\Delta_4 - \tilde{d}_4|s_4|\right) \quad \ldots (32) \\ &\quad - \frac{1}{\tau_\delta}\delta_e^2 + \frac{s_2}{r}\left(\dot{V}_{\lambda,d} - \dot{V}_{\lambda}^{*}\right) + s_3\left(\dot{\alpha}_d - \dot{\alpha}^{*}\right) + s_4\left(\dot{\omega}_{z,d} - \dot{\omega}_z^{*}\right) \\ &\quad + \frac{QSLm_{z,n}^{\delta_z}}{J_z}\bar{\delta}_z s_4 + \left|\frac{QSLm_{z,n}^{\delta_z}}{J_z}\right|\bar{\delta}_z\delta_e + \sum_{i=1}^{4}\frac{\sigma_i}{c_i}\tilde{d}_i\hat{d}_i. \end{aligned}$$

https://doi.org/10.1017/aer.2019.71 Published online by Cambridge University Press

Applying the following facts

$$\begin{cases} s_i \Delta_i \le |s_i|\,|\Delta_i| \le |s_i|\,d_i \\ -\dfrac{s_i^2 \hat{d}_i^2}{2\varepsilon_i} \le -|s_i|\,\hat{d}_i + \dfrac{\varepsilon_i}{2} \qquad i = 1, ..., 4 \\ \dfrac{\sigma_i}{c_i}\tilde{d}_i \hat{d}_i \le -\dfrac{\sigma_i}{2c_i}\tilde{d}_i^2 + \dfrac{\sigma_i}{2c_i} d_i^2 \end{cases} \quad \ldots (33)$$

to Equation (32) yields

$$\begin{aligned} \dot{V} \le & -\frac{k_1}{r}s_1^2 - \frac{k_2}{r}s_2^2 - k_3 s_3^2 - k_4 s_4^2 - \sum_{i=1}^{4}\frac{\sigma_i}{2c_i}\tilde{d}_i^2 \\ & + \sum_{i=1}^{4}\frac{\sigma_i}{2c_i}d_i^2 + \frac{\varepsilon_1+\varepsilon_1}{2r} + \frac{\varepsilon_3+\varepsilon_4}{2} \\ & + \frac{s_2}{r}\left(\dot{V}_{\lambda,d} - \dot{V}_\lambda^*\right) + s_3\left(\dot{\alpha}_d - \dot{\alpha}^*\right) + s_4\left(\dot{\omega}_{z,d} - \dot{\omega}_z^*\right) \\ & + \left|\frac{QSLm_{z,n}^{\delta_z}}{J_z}\right|\left|\bar{\delta}_z\right|\,|s_4| + \left|\frac{QSLm_{z,n}^{\delta_z}}{J_z}\right|\bar{\delta}_z\delta_e - \frac{1}{\tau_\delta}\delta_e^2 \\ \le & -\frac{k_1}{r}s_1^2 - \left(\frac{2k_2-1}{2r}\right)s_2^2 - \left(k_3 - \frac{1}{2}\right)s_3^2 - \left(k_4 - \frac{1}{2}\right)s_4^2 \\ & - \sum_{i=1}^{4}\frac{\sigma_i}{2c_i}\tilde{d}_i^2 - (k_\delta - 1)\,\delta_e^2 + \sum_{i=1}^{4}\frac{\sigma_i}{2c_i}d_i^2 + \frac{\varepsilon_1+\varepsilon_1}{2r} + \frac{\varepsilon_3+\varepsilon_4}{2} \\ & + \frac{\left(\dot{V}_{\lambda,d} - \dot{V}_\lambda^*\right)^2}{2r} + \frac{\left(\dot{\alpha}_d - \dot{\alpha}^*\right)^2}{2} + \frac{\left(\dot{\omega}_{z,d} - \dot{\omega}_z^*\right)^2}{2} \\ \le & -2\kappa_1 V + \kappa_2 + \kappa_3 \end{aligned} \quad \ldots (34)$$

where

$$\kappa_1 = \min\left\{\frac{k_1}{r}, \frac{2k_2-1}{2r}, \frac{2k_3-1}{2}, \frac{2k_4-1}{2}, \frac{\sigma_1}{2}, \frac{\sigma_2}{2}, \frac{\sigma_3}{2}, \frac{\sigma_4}{2}, k_\delta - 1\right\}$$

$$\kappa_2 = \sum_{i=1}^{4}\frac{\sigma_i}{2c_i}d_i^2 + \frac{\varepsilon_1+\varepsilon_1}{2r} + \frac{\varepsilon_3+\varepsilon_4}{2}$$

$$\kappa_3 = \frac{\left(\dot{V}_{\lambda,d} - \dot{V}_\lambda^*\right)^2}{2r} + \frac{\left(\dot{\alpha}_d - \dot{\alpha}^*\right)^2}{2} + \frac{\left(\dot{\omega}_{z,d} - \dot{\omega}_z^*\right)^2}{2}$$

According to Assumption 1, κ_1 and κ_2 are both bounded. Additionally, Theorem 1 indicates that $\left|\dot{V}_{\lambda,d} - \dot{V}_\lambda^*\right|$, $|\dot{\alpha}_d - \dot{\alpha}^*|$and $\left|\dot{\omega}_{z,d} - \dot{\omega}_z^*\right|$ are globally bounded, which means that κ_3 is also bounded. Consequently, selecting parameters $k_2 > 1/2$, $k_3 > 1/2$, $k_4 > 1/2$ and $k_\delta > 1$ yields that $\kappa_1 > 0$. With this in mind, it follows from Equation (34) that

$$0 \le V(t) \le \left(V(0) - \frac{\kappa_2+\kappa_3}{2\kappa_1}\right)e^{-2\kappa_1 t} + \frac{\kappa_2+\kappa_3}{2\kappa_1} \quad \ldots (35)$$

https://doi.org/10.1017/aer.2019.71 Published online by Cambridge University Press

Table 1
Initial parameters for simulation

Parameter	Value	Unit
The interceptor's initial position	$x_M(0) = 0$	m
	$y_M(0) = 0$	m
The velocity of the interceptor	$V_M(0) = 500$	m/s
The velocity of the target	$V_T(0) = 250$	m/s
The initial flight path angle of the interceptor	$\gamma_M(0) = 60$	Deg
The initial flight path angle of the target	$\gamma_T(0) = -160$	Deg
The initial relative range	$R(0) = 10000$	m
The initial LOS angle	$\lambda(0) = 30$	Deg
The missile initial angle-of-attack	$\alpha(0) = 0$	Deg
The missile initial pitch angular rate	$\omega_z(0) = 0$	Deg/s

which means that the error states are bounded during the convergent phase of the fixed-time differentiator.

Furthermore, as indicated in[36], the estimation errors $\left|\dot{V}_{\lambda,d} - \dot{V}_{\lambda}^{*}\right|$, $|\dot{\alpha}_d - \dot{\alpha}^{*}|$ and $\left|\dot{\omega}_{z,d} - \dot{\omega}_{z}^{*}\right|$ can converge to zero within a bounded finite time $T_{sd} > 0$, that is, $\kappa_3 = 0$ holds for all $t > T_{sd}$. Considering this, it follows from Equations (34) and (35) that when $t > T_{sd}$, the following inequality holds.

$$0 \le V(t) \le \left(V(T_{sd}) - \frac{\kappa_2}{2\kappa_1}\right) e^{-2\kappa_1 (t - T_{sd})} + \frac{\kappa_2}{2\kappa_1} \quad \ldots (36)$$

The above analysis indicates all error signals are uniformly and ultimately bounded by $\frac{\kappa_2}{2\kappa_1}$. This completes the proof of Theorem 1. Moreover, tuning design parameters appropriately, such that the upper bound $\frac{\kappa_2}{2\kappa_1}$ is arbitrarily small, helps to improve the steady performance of the proposed IGC law.

4.0 SIMULATION RESULTS

This section carries out numerical simulations to verify the performance of the proposed IGC law, where a typical air defence interception engagement is considered. The target's acceleration is assumed to be $a_T = 10\sin(0.1\pi t)$ m/s^2. The nominal aerodynamic parameters are listed as follows:

$$\begin{aligned} \frac{QSc_{y,n}^{\alpha}}{mV_M} &= 0.3487, \quad \frac{QSLm_{z,n}^{\alpha}}{J_z} = -17.801, \\ \frac{QSL^2 m_{z,n}^{\omega_z}}{J_z V_M} &= -0.2741, \quad \frac{QSLm_{z,n}^{\delta_z}}{J_z} = -56.267. \end{aligned} \quad \ldots (37)$$

The aerodynamic coefficients are assumed to have 30% uncertain variations with respect to their nominal values in this paper. The maximum of the fin deflection angle is $\delta_{\max} = 30$ Deg. The initial conditions of the interceptor and the target are given in Table 1.

https://doi.org/10.1017/aer.2019.71 Published online by Cambridge University Press

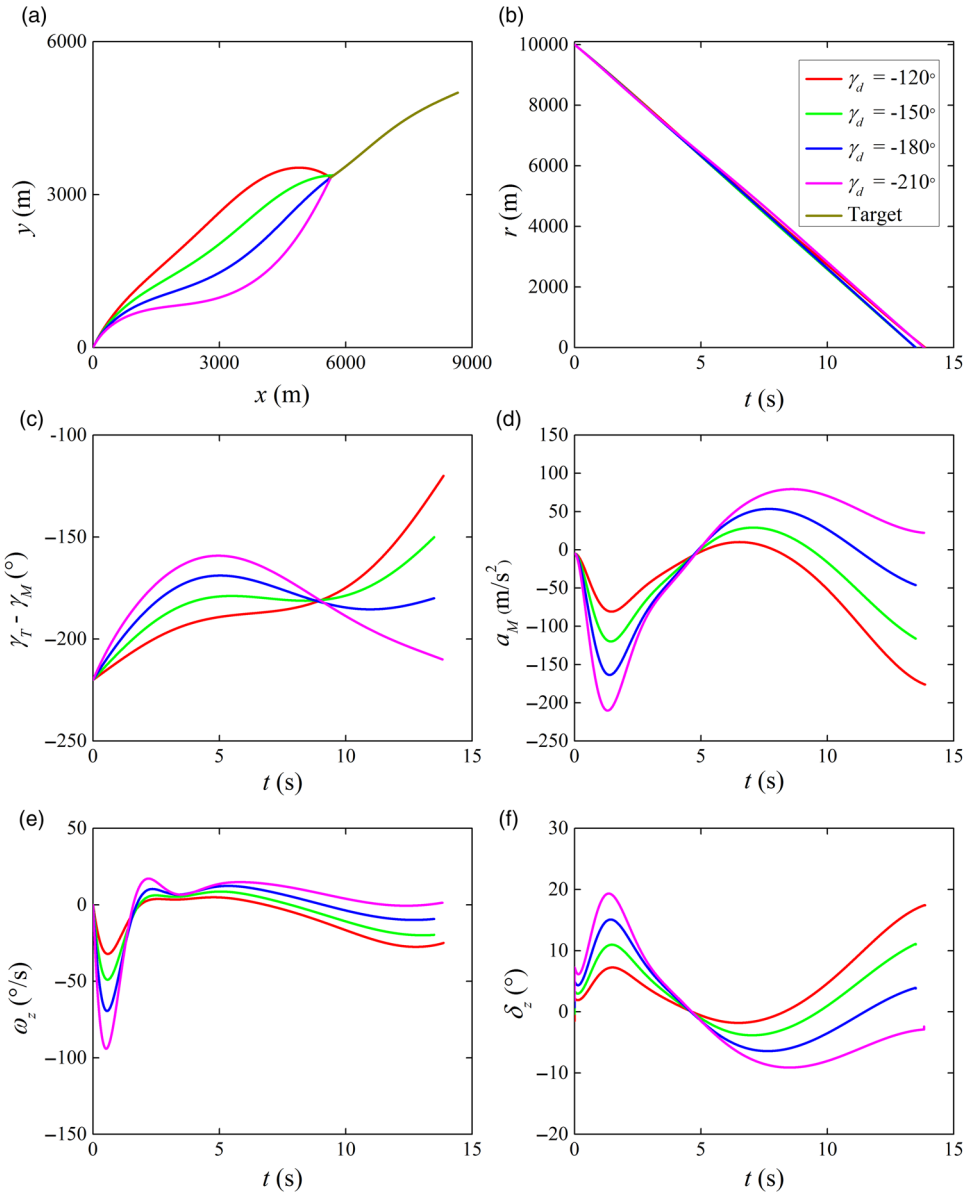

Figure 3. Simulation results with various desired impact angles: (a) interception trajectories, (b) relative distances, (c) LOS angles, (d) missile achieved accelerations, (e) pitch angular rates and (f) fin deflections.

4.1 Interception with different desired impact angles

In this case, the simulation results of weaving target interception with various desired impact angles are investigated. The desired impact angles γ_d are chosen as -120 Deg, -150 Deg, -180 Deg and -210 Deg, respectively. The simulation results are shown in Fig. 3. The terminal miss distance and impact angle error are presented in Table 2. It follows from Table 2 and Fig. 3 that small acceptable miss distances and impact angle errors are obtained by

https://doi.org/10.1017/aer.2019.71 Published online by Cambridge University Press

Table 2
Miss distance and impact angle error

γ_d (Deg)	Miss distance (m)	Impact angle error (Deg)
−120	0.40519	0.00167
−150	0.29176	0.00481
−180	0.11990	0.00058
−210	0.13044	0.00083

the proposed IGC law for impact angle constrained target capture. Specifically, the impact angle error and the miss distance are less than 0.005 Deg and 0.5 m, respectively. Also, it can be seen from Fig. 3 that fin deflection angle command is within the allowable maximum value and quite smooth during the homing engagement. Consequently, hard constraints on the impact angle error and miss distance are both guaranteed by the proposed IGC law against an unknown-manoeuvring target with the limit of actuator resource.

4.2 Comparison with the NTSM law

To evaluate the superiority of the proposed IGC law, a comparison simulation with the well-known NTSM law is carried out in this case. The NTSM law is defined as

$$\begin{aligned} s &= (\lambda - \lambda_d) + \beta \left(\dot{\lambda} - \dot{\lambda}_d\right)^{\alpha}, \ \alpha = \frac{p}{q}, \ p > q \\ a_M &= \frac{r}{\cos(\gamma_M - \lambda)} \left(-\frac{2\dot{r}\dot{\lambda}}{r} + \frac{1}{\alpha\beta}\dot{\lambda}^{(2-\alpha)} \right) + \frac{\varepsilon sgn(s)}{sgn(\cos(\gamma_M - \lambda))} \end{aligned} \quad \ldots (38)$$

where $\beta > 0$ and $\varepsilon > 0$ are design gains; p and q are two positive odd integers, such that $1 < \alpha < 2$. To improve the performance of the NTSM law, it is assumed that the desired acceleration a_M generated by the NTSM law can be produced without any autopilot lag. Whereas the proposed IGC law acts on the missile dynamics in Equation (7). The acceleration limit is considered as $|a_M| \leq 200\,\mathrm{m/s^2}$ for the NTSM method. The desired impact angle is selected as $\gamma_d = -160$Deg.

Figure 4 illustrates the simulation results in detail. It can be seen from this figure that both the proposed IGC law and the well-known NTSM approach can successfully navigate the missile to attack the target with desired impact angle; however, the proposed IGC law achieves better accuracy with relatively less acceleration than the NTSM law. Moreover, Equation (38) indicates that the NTSM law requires the acceleration information of the target in sliding surface design, which may not be suitable for practical applications because the future action of the target usually cannot be predicted beforehand. Compared with the NTSM method, the introduction of the adaptive law in the IGC law design contributes to overcome this drawback effectively.

5.0 CONCLUSIONS

This study considers the full impact angle constrained IGC law design problem for manoeuvring target interception with actuator saturation. By regarding the target acceleration and aerodynamic uncertainties as lumped disturbances, an adaptation law is proposed to estimate the upper bound of the disturbances. Based on the adaptation law, the proposed IGC law is preformed via the typical backstepping process, where a fixed-time differentiator is introduced

https://doi.org/10.1017/aer.2019.71 Published online by Cambridge University Press

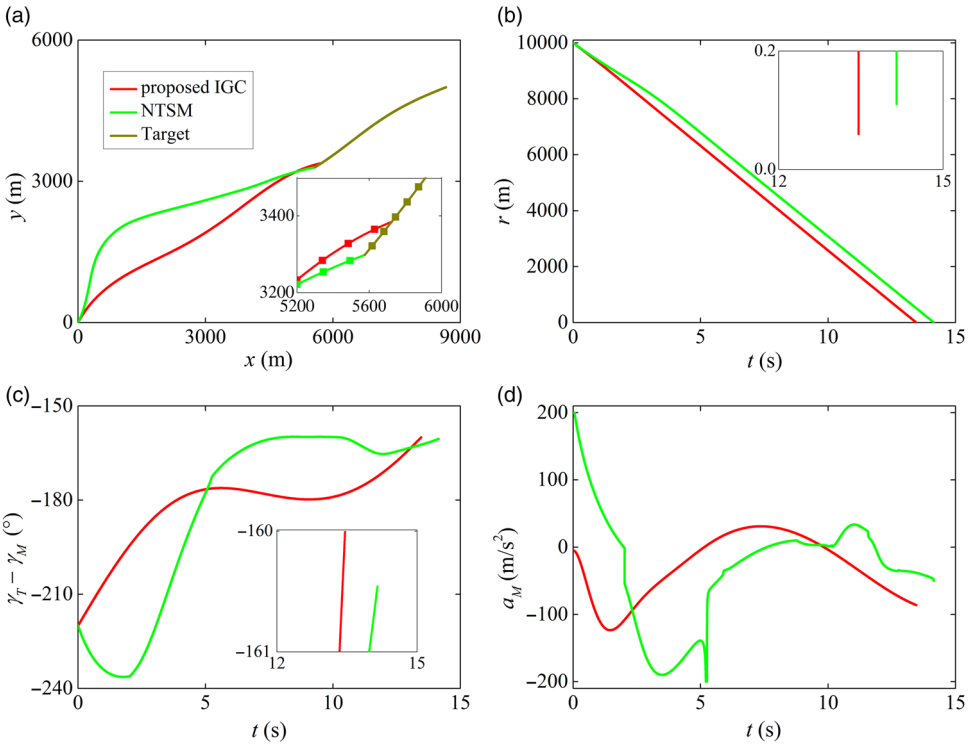

Figure 4. Comparison results with the NTSM law: (a) interception trajectories, (b) relative distances, (c) LOS angles and (d) missile achieved accelerations.

to avoid the problem of 'explosion of complexity'. Moreover, an auxiliary first-order filter is also presented to cope with the actuator saturation problem. Stability analysis is carried out by selecting a typical Lyapunov function candidate. Simulation results with comparison examples are given to demonstrate the superiority of the proposed integrated guidance and control law.

Supplementry Material

To view supplementary material for this article, please visit https://doi.org/10.1017/aer.2019.71.

REFERENCES

1. YAN, H., TAN, S. and HE, Y. A small-gain method for integrated guidance and control in terminal phase of re-entry. *Acta Astronaut*, 2017, **132**, pp 282–292.
2. WANG, X. and WANG, J. Partial integrated guidance and control with impact angle constraints. *J Guidance Control Dyn*, 2015, **38**, (5), pp 925–936.
3. YANG, C. and YANG, C. Analytical solution of three-dimensional realistic true proportional navigation. *J Guidance Control Dyn*, 2012, **19**, (3), pp 569–577.
4. OHIMEYER, E. Root-mean-square miss distance of proportional navigation missile against sinusoidal target. *J Guidance Control Dyn*, 2015, **19**, (3), pp 563–568.

https://doi.org/10.1017/aer.2019.71 Published online by Cambridge University Press

5. ZHOU, D., MU, C. and XU, W. Adaptive sliding-mode guidance for a homing missile. *J Guidance Control Dyn*, 1999, **22**, (4), pp 589–594.
6. MOON, J., KIM, K. and KIM, Y. Design of missile guidance law via variable structure control. *J Guidance Control Dyn*, 2001, **24**, (4), pp 659–664.
7. LECHEVIN, N. and RABBATH, C. Lyapunov-based nonlinear missile guidance. *J Guidance Control Dyn*, 2004, **27**, (3), pp 1096–1102.
8. SHIMA, T. Intercept-angle guidance. *J Guidance Control Dyn*, 2011, **34**, (2), pp 484–492.
9. KUMAR, S., RAO, S. and GHOSE, D. Sliding-mode guidance and control for all-aspect interceptors with terminal angle constraints. *J Guidance Control Dyn*, 2012, **35**, (4), pp 1230–1246.
10. KUMAR, S., RAO, S. and GHOSE, D. Non-singular terminal sliding mode guidance with impact angle constraints. *J Guidance Control Dyn*, 2014, **37**, (4), pp 610–621.
11. ZHANG, Y., TANG, S. and GUO, J. Adaptive terminal angle constraint interception against manoeuvring targets with fast fixed-time convergence. *Int J Robust Nonlinear Control*, 2018, **28**, pp 2996–3014.
12. ZHANG, Y., TANG, S. and GUO, J. An adaptive fast fixed-time guidance law with an impact angle constraint for intercepting manoeuvring targets. *Chinese J Aeronaut*, 2018, **31**, (6), pp 1327–1344.
13. GURFIL, P., JODORKOVSKYM, M. and GUELMAN, M. Finite time stability approach to proportional navigation systems analysis. *J Guidance Control Dyn*, 1998, **21**, (6), pp 853–861.
14. CHWA, D. and CHOI, J. Adaptive nonlinear guidance law considering control loop dynamics. *IEEE Trans Aerosp Electron Syst*, 2003, **39**, (40), pp 1134–1143.
15. SUN, S., ZHOU, D. and HOU, W. A guidance law with finite time convergence accounting for autopilot lag. *Aerosp Sci Technol*, 2013, **25**, (1), pp 132–137.
16. HE, S., LIN, D. and WANG, J. Robust terminal angle constraint guidance law with autopilot lag for intercepting manoeuvring targets. *Nonlinear Dyn*, 2015, **81**, (1), pp 881–892.
17. ZHOU, D., QU, P. and SUN, S. A guidance law with terminal impact angle constraint accounting for missile autopilot. *J Dyn Syst Meas Control*, 2013, **135**, (5), pp 1–10.
18. MENON, P. and OHLMEYE, R.E. Integrated design of agile missile guidance and autopilot systems. *Control Eng Practice*, 2001, **9**, (10), pp 1095–1106.
19. VADDO, S., MENON, P. and OHLMEYE, R.E. Numerical state-dependent Raccati equation approach for missile integrated guidance control. *J Guidance Control Dyn*, 2009, **32**, (2), pp 699–703.
20. XIN, M., BALAKRISHNAN, S. and OHLMEYER, E . Integrated guidance and control missiles with $\theta - D$ method. *IEEE Trans Control Syst Technol*, 2006, **14**, (6), pp 981–992.
21. PADHI, R., CHAWLA, C. and DAS, P. Partial integrated guidance and control of interceptors for high-speed ballistic targets. *J Guidance Control Dyn*, 2014, **37**, (1), pp 149–163.
22. KIM, J., WHANG, I. and KIM, B. Finite horizon integrated guidance and control for terminal homing in vertical plane. *J Guidance Control Dyn*, 2016, **39**, (5), pp 1104–1112.
23. HE, S., LIN, D. and WANG, J. Continuous second-order sliding mode based impact angle guidance law. *Aerosp Sci Technol*, 2015, **41**, pp 199–208.
24. SHIMA, T., IDAN, M. and GOLAN, O. Sliding-mode control for integrated missile autopilot guidance. *J Guidance Control Dyn*, 2006, **29**, (2), pp 250–260.
25. IDAN, M., SHIMA, T. and GOLAN, O . Integrated sliding mode autopilot-guidance for dual-control missiles. *J Guidance Control Dyn*, 2007, **30**, (4), pp 1081–1089.
26. SHIN, H., HWANG, T., TSOPURDOS, A., WHITE, B. and TAHK, M. Integrated intercept missile guidance and control with terminal angle constraint. Proceedings of the 26th International Congress of the Aeronautical Sciences, 2008, IEEE, pp 1875–1884.
27. YAN, H., WANG, W., YU, B. and JI, H. Adaptive integrated guidance and control based on backstepping and input-to-state stability. *Asian J Control*, 2014, **16**, (2), pp 602–608.
28. SHEN, Y., YU, J., LUO, G., AI, X. and JIA, Z. Observer-based adaptive sliding mode backstepping output-feedback DSC for spin-stabilised canard-controlled projectiles. *Chinese J Aeronaut*, 2017, **30**, (3), pp 1115–1126.
29. HOU, M., LIANG, X. and DUAN, G. Adaptive block dynamic surface control for integrated missile guidance and autopilot. *Chinese J Aeronaut*, 2013, **26**, (3), pp 741–750.
30. RAN, M., WANG, Q., HOU, D. and DONG, C. Backstepping design of missile guidance and control based on adaptive fuzzy sliding mode control. *Chinese J Aeronaut*, 2014, **27**, (3), pp 634–642.
31. HE, S., SONG, T. and LIN, D. Impact angle constrained integrated guidance and control for manoeuvring target interception. *J Guidance Control Dyn*, 2017, **40**, (10), pp 2652–2660.

https://doi.org/10.1017/aer.2019.71 Published online by Cambridge University Press

32. WANG, X., ZHENG, Y. and LIN, H. Integrated guidance and control law for cooperative attack of multiple missiles. *Aerosp Sci Technol*, 2015, **42**, pp 1–11.
33. WANG, W., XIONG, S., WANG, S., SONG, S. and LAI, C. Three dimensional impact angle constrained integrated guidance and control for missiles with input saturation and actuator failure. *Aerosp Sci Technol*, 2016, **53**, pp 169–187.
34. HE, S., WANG, W. and WANG, J. Three-dimensional multivariable integrated guidance and control design for maneuvering targets interception. *J Franklin Inst*, 2016, **353**, pp 4330–4350.
35. HE, S., WANG, W. and WANG, J. Adaptive backstepping impact angle control with autopilot dynamics and acceleration saturation consideration. *Int J Robust Nonlinear Control*, 2017, **27**, pp 3777–3893.
36. BASIN, M., YU, P. and SHTESSEL, Y. Finite- and fixed-time differentiators utilising HOSM techniques. *IET Control Theory Appl*, 2017, **11**, (8), pp 1144–1152.

https://doi.org/10.1017/aer.2019.71 Published online by Cambridge University Press